Electronic Supplementary Material (ESI) for Energy Advances.

Supplementary Information

Effect of Doping TiO_2 with Mn for Electrocatalytic Oxidation in Acid and Alkaline Electrolytes

Lauren Vallez[1#], Santiago Jimenez-Villegas[2#], Angel T. Garcia-Esparza[3#], Yue Jiang[1], Sangwook Park[4,5,6], Qianying Wu[1], Thomas Mark Gill[7], Dimosthenis Sokaras[3*], Samira Siahrostami[2*], and Xiaolin Zheng[1*]

[1]Department of Mechanical Engineering, Stanford University, Stanford, California 94305, USA
[2]Department of Chemistry, University of Calgary, 2500, University Drive NW, Calgary, Alberta, Canada T2N 1N4
[3]Stanford Synchrotron Radiation Lightsource, SLAC National Accelerator Laboratory, 2575 Sand Hill Road, Menlo Park, USA
[4]Department of Mechanical Engineering, Seoul National University, Seoul 08826, South Korea
[5]Institute of Advanced Machines and Design, Seoul National University, Seoul 08826, South Korea
[6]Institute of Engineering Research, Seoul National University, Seoul 08826, South Korea
[7]Department of Chemical Engineering, Massachusetts Institute of Technology, Cambridge, MA 02139, USA

[#]These authors contributed equally
[3*]Dimosthenis Sokaras corresponding author e-mail address: dsokaras@slac.stanford.edu
[2*]Samira Siahrostami corresponding author e-mail address: samira.siahrostami@ucalgary.ca
[1*]Xiaolin Zheng corresponding author e-mail address: xlzheng@stanford.edu

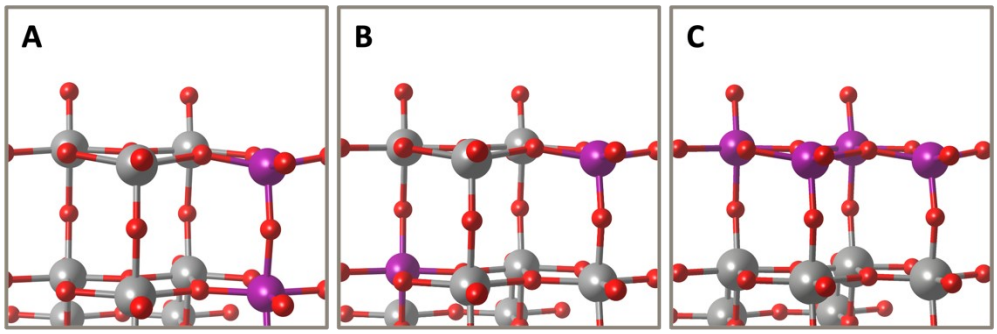

Figure S1. Side view of the optimized structures of **(A)**, **(B)** Mn incorporation into the surface and subsurface of TiO_2 (101), and **(C)** fully Mn-saturated surface layer of TiO_2 (101). Grey, purple, and red spheres represent Ti, Mn, and O atoms, respectively.

Density functional theory was used to determine the adsorption free energies, ΔG, of the 4e-WOR reaction intermediates (O*, OH*, and OOH*). ΔG was calculated at zero potential and pH=0, using the following equation: $\Delta G = \Delta E + \Delta ZPE - T\Delta S$, where ΔE, ΔZPE, and ΔS are adsorption energies with respect to water, zero-point energy difference, and change in entropy, respectively. ΔZPE and ΔS were obtained from ref. [1] Additionally, the computational hydrogen electrode model (CHE) was used. This approach assumes the chemical potential of a proton-electron pair to be equal to that of gas-phase H_2 at $U_{elec}=0.0$ V vs. the reversible hydrogen electrode (RHE).[1] By shifting the electron energy by $-eU_{elec}$ when e and U_{elec} are the elementary charge and electrode potential, respectively, the effect of the electrode potential is taken into account.

To gain a better understanding of the nature of the Mn-oxygen intermediate interaction, a Bader charge analysis was carried out on the Mn and Ti active sites via the Bader analysis program in VASP developed by Henkelman et al.[2] **Figure S2** shows the Bader analysis on the Mn and Ti active site on Mn:TiO_2 and TiO_2 (101) in the presence/absence of OH*, O*, and OOH* adsorbates. Contrasting both the Mn and Ti active sites, a greater change in net effective charges is observed on the Mn than on the Ti when an oxygen intermediate is adsorbed on the surface (i.e., M-O*). For instance, the Bader charge on the Mn and Ti atoms are calculated to be 1.67 $|e|$ and 1.92 $|e|$, respectively. When OH* is adsorbed on the surface, a change in effective charge of 0.082 $|e|$ and 0.051$|e|$, is calculated for the Mn and Ti sites, respectively. This is evidence of a stronger charge transfer between Mn and the adsorbate when compared to that between the Ti and adsorbate. This charge transfer between metal site and O* species is further observed in the oxygen Bader charge. The Bader charge on the O* in all the reaction intermediates becomes less negative when adsorbed on Mn rather than on the Ti site. A more positive Bader charge on O combined with a greater, negative, change in Mn charge suggests a preferential metal-oxygen (M-O) bond, relative to that observed in Ti-O*. This is in well-agreement with our adsorption free energy calculations, in which the presence of an Mn active site lowers the ΔG of reaction intermediates, reflecting a stronger M-O bond.

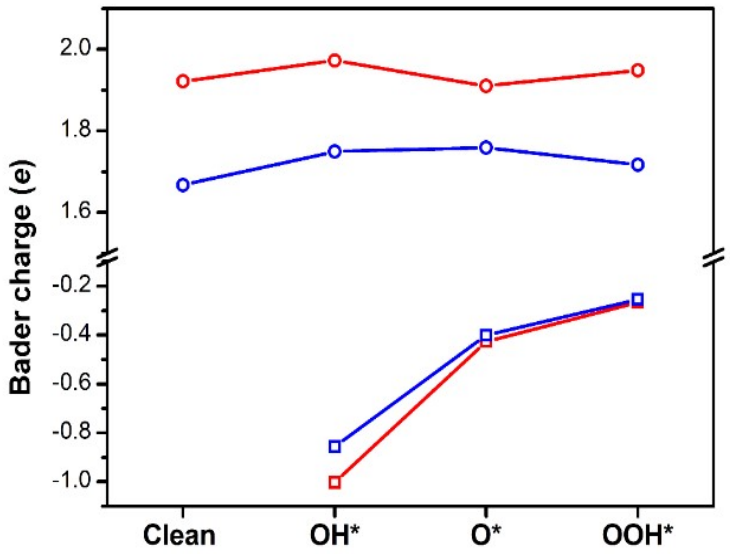

Figure S2. Bader charge analysis carried out on the Mn:TiO_2 (blue) and TiO_2 (101) (red) structures. Circle data points represent the Bader charge on the metal active site (i.e., Mn and Ti) with and without adsorbed species (OH*, O*, and OOH*). Square points represent the Bader charge on the oxygen atom of the oxygen-containing WOR intermediates when adsorbed on the Mn or Ti active site.

The results from the Bader charge analysis are further supported by the charge density difference plot of the oxygen-containing molecule on the Mn and Ti sites. We consider the adsorption of OH* on the surface of TiO_2 (101) and Mn:TiO_2 as a model for the charge density difference investigation (**Figure S3**). The plot shows that on the Mn site, O interacts with the metal through its bonding state, whereas on the Ti the interaction occurs via an antibonding state. A large charge exchange cloud is observed between the adsorbed OH* and the Mn active site, whilst the Ti-OH* lacks this feature. As the binding event of the reaction intermediate is often accompanied by redistribution in charge, the strength of the M-O interaction can be qualitatively assessed from the size of the charge exchange cloud. Hence, our previous results are sustained by the charge density difference plot; adsorption of $4e^-$ WOR intermediates is preferred on the Mn site over Ti.

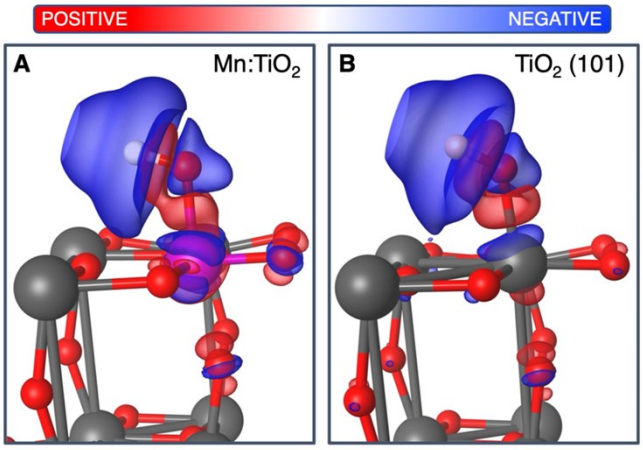

Figure S3. Differential charge density plots illustrating the distribution of electrons on (A) Mn:TiO_2, and (B) TiO_2 (101) surfaces upon adsorption of OH* intermediate. Blue and red regions represent electron accumulation and depletion, respectively. Grey, purple, white, and red spheres represent Ti, Mn, H, and O atoms, respectively.

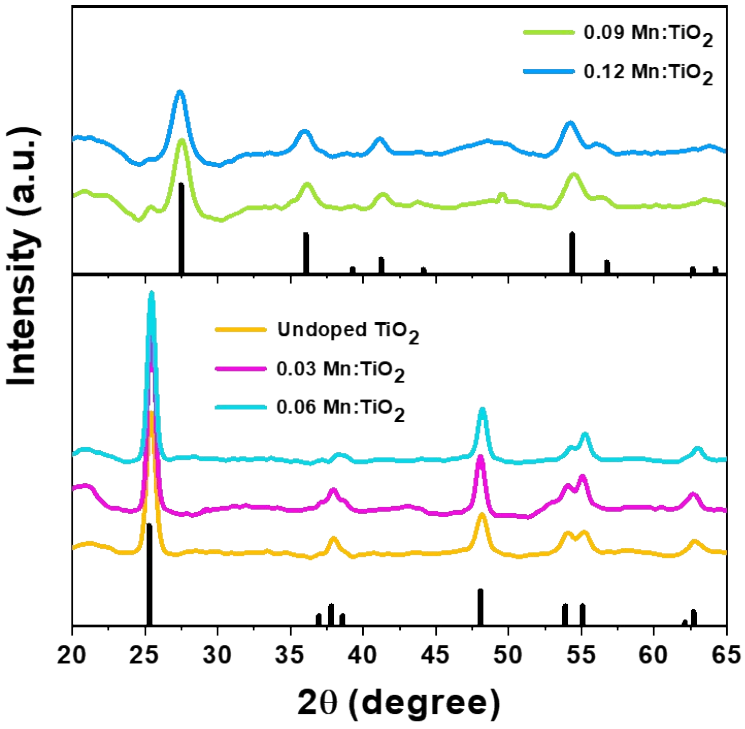

Figure S4. Top: XRD spectra of 0.09 and 0.12 Mn:TiO_2 with rutile TiO_2 reference peaks. Bottom: XRD spectra of undoped, 0.03, and 0.06 Mn:TiO_2 with anatase TiO_2 reference peaks.

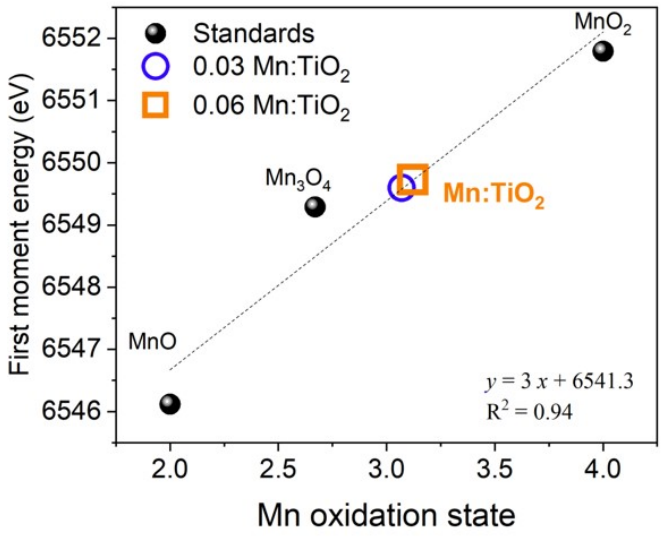

Figure S5. Mn K-edge X-ray absorption near edge structure (XANES) first-moment analysis. The first-moment analysis of the Mn K-edge XANES shows that Mn atoms in 0.03 and 0.06 Mn:TiO_2 samples have an average oxidation state of 3.1. The XANES spectra of reference standards are shown for comparison (MnO, Mn_3O_4, and MnO_2).

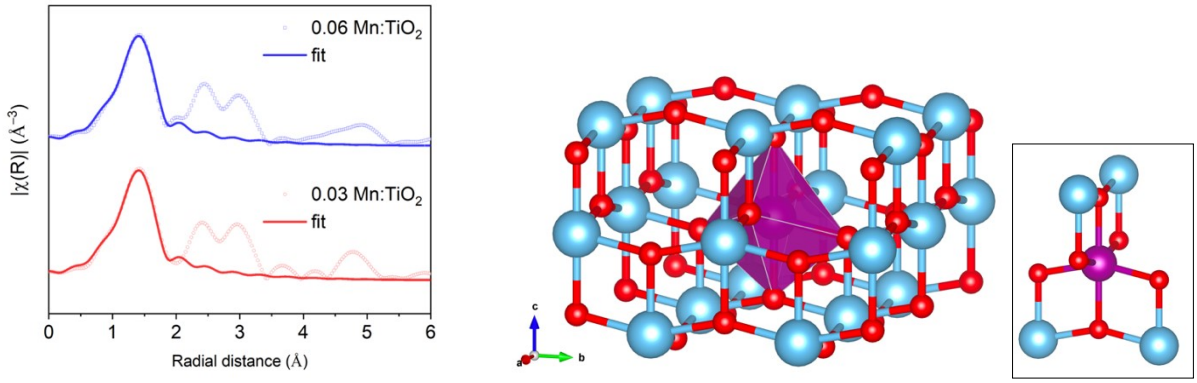

Figure S6. Analysis of the first shell Mn K-edge FT-EXAFS of the 0.03 and 0.06 Mn:TiO_2 doped samples. Symbols show the experimental data and the solid lines are the theoretical fittings. The theoretical model used for the FT-EXAS fitting with a closer look to the atomic environment of the Mn atom substituting Ti in anatase. The Ti atoms in blue, Mn atoms in purple, and Oxygen atoms in red.

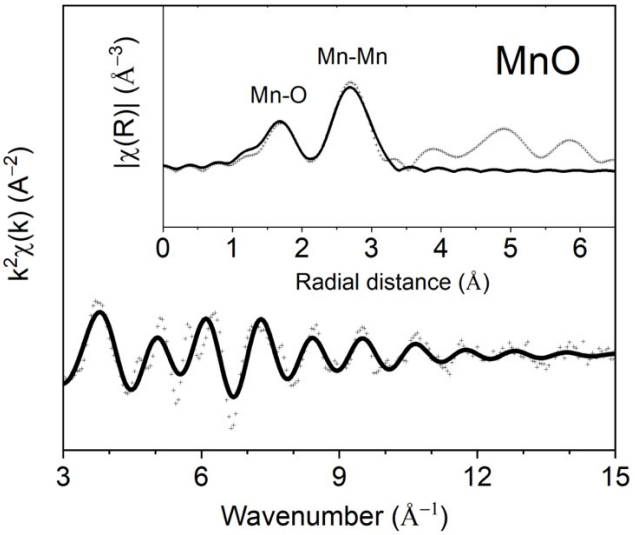

Figure S7. Mn K-edge extended X-ray absorption fine structure (EXAFS) and the inset shows the Fourier-transformed EXAFS (FT-EXAFS) of the MnO oxide reference standard. Symbols show the experimental data and the solid lines are the theoretical fittings.

Table S1. First-shell Mn K-edge FT-EXAFS fitting parameters of 0.03 and 0.06 Mn:TiO_2 samples. First, we assume that the Mn substitutes a Ti atom in the anatase lattice. We also reasonably assume that the Mn sites' chemical environments in the 0.03 and the 0.06 Mn:TiO_2 samples are similar (based on the XRD results and the XANES spectra in **Figure 4a**). Parentheses show one standard deviation for the last digit. Underlined numbers show fixed values. Multiple dataset fitting, multiple k-weight fitting, amplitude fixed at 0.6, Hanning window, dk = 1, *k* range of 3-10.5 $Å^{-1}$, and R-range of 1.0-1.8. The R-factor metric can be considered here as a measure of the percentage of misfit between the data and theory.

	Path		**CN**			**σ^2 ($Å^2$)**			**ΔE^0**		**R (Å)**		**R-factor**
0.03 and 0.06													
Mn:TiO_2	Mn–O		5.8	(4)		0.008	(1)		-7 (1)		1.91 (1)		0.0036

Table S2. Mn K-edge Fourier FT-EXAFS fitting parameters of the MnO standard. FT-EXAFS in R space in **Figure S6** were fitted using the Artemis software with a Kaisser-Bessel window, dk = 1, *k* range of 3-10.0 $Å^{-1}$ for MnO and R-range of 1.4-3.2. The structure of the MnO standard was obtained from the ICSD database. Parentheses show one standard deviation for the last digit. The fitting parameters include the path, the coordination number (CN), the interatomic distance (R), the mean-square deviation in R (σ^2), and the energy shift parameter (ΔE).

	Path		**CN**			**σ^2 ($Å^2$)**			**ΔE^0**		**R (Å)**		**Amplitude**	**R-factor**
MnO	Mn–O		6			0.008	(4)		2	(1)	2.19	(2)	0.6 (1)	0.012
	Mn–Mn		12			0.007	(2)				3.14	(1)		

Table S3. Long-range FT-EXAFS analysis of 0.03 and 0.06 Mn:TiO_2 samples assuming Mn substitution in the anatase lattice. The fitting was performed assuming that all parameters are equal in both samples with the anatase structure obtained from the ICSD database ($I4_1/amdZ$ space group). Multiple dataset fitting, multiple k-weight fitting, amplitude fixed at 0.6, Hanning window, dk = 1, *k* range of 3-10.5 $Å^{-1}$, and R-range of 1.0-3.7. The $CN_{Mn\text{-}Ti}$ = 1.8 is lower than the expected value of 4 for bulk anatase. The longer scattering path's coordination numbers are in reasonable agreement with the expected anatase values of 4 and 16 for Mn-O-Ti and Mn-O', respectively. An attempt to use a longer Mn-Ti' scattering path instead of the Mn-O-Ti multiple scattering resulted in unphysical parameters; similarly, an attempt to use Mn-O-Mn multiple scattering or Mn-Mn' scattering paths also resulted in unphysical parameters.

	Path		**CN**			**σ^2 ($Å^2$)**			**ΔE^0**		**R (Å)**		**R-factor**
0.03 and 0.06													
Mn:TiO_2	Mn–O		5.9	(3)		0.0080	(8)		-8.5 (7)		1.902 (4)		0.0088
	Mn–Ti		1.8	(7)		0.008	(3)				2.89 (1)		
	Mn–O–Ti		3	(2)		0.001	(4)				3.76 (2)		
	Mn–O'		16	(1)		0.0080	(8)				3.95 (3)		

Table S4. FT-EXAFS analysis of 0.03 and 0.06 Mn:TiO_2 samples assuming Mn substitution in the DFT-optimized (101) terminated anatase surface. A DFT-optimized anatase TiO_2(101) surface model with one Mn substituting the Ti atom on the surface was utilized as a model for the EXAFS fit. Similar scattering paths were employed for consistency with the bulk anatase model. In this case, the Mn on the surface is expected to present a lower Mn-Ti coordination number of 3. Parentheses show one standard deviation for the last digit. Underlined numbers show fixed values. Multiple dataset fitting, multiple k-weight fitting, amplitude fixed at 0.6, Hanning window, dk = 1, k range of 3-10.5 $Å^{-1}$, and R-range of 1.0-3.7. The overall misfit decreased when compared to the bulk anatase fitting, and the obtained parameters remained consistent under the fit's assumption that the 0.03 and 0.06 samples contain Mn in a similar environment.

	Path		**CN**			**σ^2 ($Å^2$)**			**ΔE^0**		**R (Å)**		**R-factor**
0.06 Mn:TiO_2(101)	Mn–O		5.7	(4)		0.008	(1)		-8.4 (8)		1.900 (5)		0.0075
	Mn–Ti		1.3	(4)		0.005	(3)				2.88 (1)		
	Mn–O–Ti		6	(1)		0.005	(3)				3.78 (1)		
	Mn–O'		15	(2)		0.008	(1)				3.99 (2)		
0.03 Mn:TiO_2(101)	Mn–O		5.9	(5)		0.008	(1)		-9 (1)		1.903 (9)		
	Mn–Ti		1.1	(5)		0.005	(3)				2.89 (2)		
	Mn–O–Ti		7	(1)		0.005	(3)				3.78 (2)		
	Mn–O'		17	(3)		0.008	(1)				3.99 (3)		

Table S5. FT-EXAFS analysis of 0.03 and 0.06 Mn:TiO_2 samples assuming Mn substitution in the DFT-optimized (001) terminated anatase surface. A DFT-optimized anatase TiO_2(001) surface model with one Mn substituting the Ti atom on the surface was utilized as a model. In this case, the Mn on the surface is expected to have a lower Mn-Ti coordination number of 2 (at ≈ 3 Å). Although the DFT model does not include either Mn-O or Mn-OH terminated functional groups at the surface, we have used the resolved first octahedral shell with 5.8 Oxygen atoms around the Mn atom to decrease the uncertainty (i.e., result from **Figure S5 and Table S1**). Parentheses show one standard deviation for the last digit. Multiple dataset fitting, multiple k-weight fitting, amplitude fixed at 0.6, Hanning window, dk = 1, *k* range of 3-10.5 $Å^{-1}$, and R-range of 1.0-3.71. The fit shows that the CN_{Mn-Ti} range is between 1.3 and 1.7. The other CNs are in reasonable agreement with the assumed geometric structure. Consistent results are obtained with both bulk and surface anatase models. The fitting with the lowest misfit (i.e., R-factor value) is presented in **Figure 4c**.

	Path		**CN**			**σ^2 ($Å^2$)**			**ΔE^0**		**R (Å)**		**R-factor**
0.06 Mn:TiO_2(001)	Mn–O		5.8			0.008			-9.0 (3)		1.9		0.0073
	Mn–Ti		1.7	(5)		0.007	(3)				2.885 (8)		
	Mn–O–Ti		4	(2)		0.002	(4)				3.77 (1)		
	Mn–O’		15	(1)		0.008					3.97 (3)		
0.03 Mn:TiO_2(001)	Mn–O		5.8			0.008			-9.7 (6)		1.9		
	Mn–Ti		1.3	(5)		0.007	(3)				2.89 (2)		
	Mn–O–Ti		4	(2)		0.002	(4)				3.76 (2)		
	Mn–O’		17	(2)		0.008					3.97 (3)		

References

1 J. K. Nørskov, J. Rossmeisl, A. Logadottir, L. Lindqvist, J. R. Kitchin, T. Bligaard and H. Jónsson, *J. Phys. Chem. B*, 2004, **108**, 17886–17892.

2 W. Tang, E. Sanville and G. Henkelman, *J. Phys. Condens. Matter*, , DOI:10.1088/0953-8984/21/8/084204.